Di-n-butyl[N′-(3-methoxy-2-oxidobenzylidene)-N-phenylcarbamohydrazonothioato]tin(IV): crystal structure, Hirshfeld surface analysis and computational study

Enis Nadia Md Yusof,[a,b] Huey Chong Kwong,[c] Thiruventhan Karunakaran,[d,e] Thahira B. S. A. Ravoof[b,f]‡ and Edward R. T. Tiekink[c]*

[a]Chemistry Section, School of Distance Education, Universiti Sains Malaysia, 11800 USM, Pulau Pinang, Malaysia, [b]Department of Chemistry, Faculty of Science, Universiti Putra Malaysia, UPM Serdang 43400, Malaysia, [c]Research Centre for Crystalline Materials, School of Medical and Life Sciences, Sunway University, 47500 Bandar Sunway, Selangor Darul Ehsan, Malaysia, [d]Centre for Drug Research, Universiti Sains Malaysia, 11800 Minden, Pulau Pinang, Malaysia, [e]School of Chemical Sciences, Universiti Sains Malaysia, 11800 USM, Pulau Pinang, Malaysia, and [f]Foundry of Reticular Materials for Sustainability (FORMS), Materials Synthesis and Characterization Laboratory, Institute of Advanced Technology, Universiti Putra Malaysia, 43400 Serdang, Selangor Darul, Ehsan, Malaysia. *Correspondence e-mail: edwardt@sunway.edu.my

The title diorganotin Schiff base derivative, $[Sn(C_4H_9)_2(C_{15}H_{13}N_3O_2S)]$, features a penta-coordinated tin centre defined by the N,O,S-donor atoms of the di-anionic Schiff base ligand and two methylene-C atoms of the n-butyl substituents. The resultant C_2NOS donor set defines a geometry intermediate between trigonal–bipyramidal and square-pyramidal. In the crystal, amine-N—H···O(methoxy) hydrogen bonding is found in a helical, supramolecular chain propagating along the b-axis direction. The chains are assembled into a layer parallel to ($\bar{1}01$) with methylene-C—H···π(phenyl) interactions prominent; layers stack without directional interactions between them. The analysis of the calculated Hirshfeld surface showed the presence of weak methylene-C—H···π(phenyl) interactions and short H···H contacts in the inter-layer region. Consistent with the nature of the identified contacts, the stabilization of the crystal is dominated by the dispersion energy term.

1. Chemical context

Thiosemicarbazones are an important class of compounds that have received wide attention due to their many biological and pharmacological properties, such as anti-bacterial, anti-viral, anti-neoplastic and anti-malarial activities (Kovala-Demerzi et al., 1997; Hu et al., 2006; Khan & Yusuf, 2009). Thiosemicarbazone Schiff bases are similar to their dithiocarbazate counterparts in that complexation with a metal centre is achieved via the nitrogen and sulfur atoms following deprotonation of the S—H and N—H groups (Đilović et al., 2008; Wiecek et al., 2009; Pavan et al., 2010; Parrilha et al., 2011; Singh et al., 2016; Palanimuthu et al., 2017). Tin(IV) compounds of 3-methoxysalicylaldehyde thiosemicarbazone have been evaluated for their in vitro cytotoxicity against a line of human T lymphocyte cells, Jurkat cells (Khandani et al., 2013): in this study, a structure–activity analysis for the di-alkyltin(IV) compounds indicated that cytotoxicity increased with the length of the alkyl carbon chain of the tin-bound substituents. Thus, the cytotoxicity was in the order of dibutyl > diphenyl > dimethyl (Khandani et al., 2013). The ability of
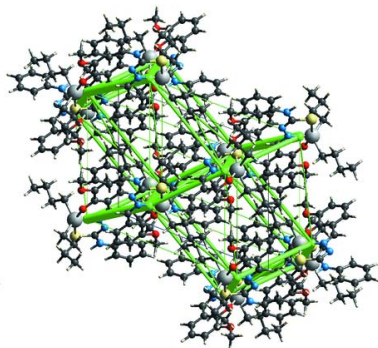
the 2-acetylpyridine *N*(4)-cyclohexylthiosemicarbazone Schiff base (*L*H$_2$) and its distorted pentagonal bipyramidal tin(IV) compound, [Ph$_2$Sn(*L*)(OAc)]·EtOH, to inhibit tumour cell growth against HepG2 cells has also been reported (Liu *et al.*, 2017). This study showed the tin(IV) compound to exhibit threefold higher cytotoxic potency compared to the free ligand, *i.e.* with IC$_{50}$ values of 3.32±0.52 and 10.10±2.07 µ*M*, respectively, and to be more potent than the reference drug mitoxantone (IC$_{50}$ = 5.3±2.38 µ*M*). Significant activity was also observed in an *in vitro* cytotoxic assay of tin(IV) compounds of 2-hydroxy-5-methoxybenzaldehyde-*N*(4)-methylthiosemicarbazone (Salam *et al.*, 2016), diphenyltin(IV) compounds of 2-benzoylpyridine *N*(4)-phenyl thiosemi-carbazone and 2-acetylpyrazine *N*(4)-phenylthiosemi-carbazone (Li *et al.*, 2011) in comparison to the standard drugs used. It may be concluded that the coordination of the Schiff base ligand to the tin(IV) centre enhanced cytotoxic activity, where the reported IC$_{50}$ values were better than standard drugs.
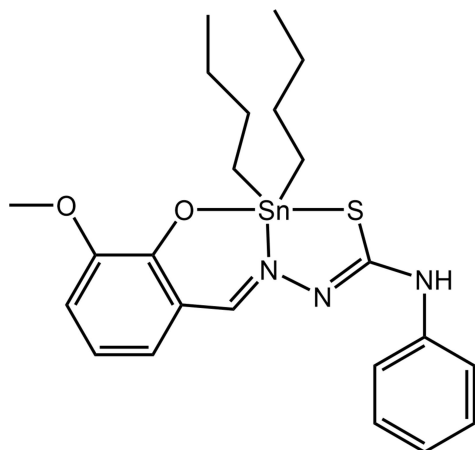
Further, the enhancement of cytotoxicity in the diphenyltin derivatives has been attributed to the presence of these phenyl groups, which suggested interactions between the tin-bound phenyl groups with intra-cellular biomacromolecules. An independent biological study suggested that the diffusion, lipophilic character and steric effects associated with the ligand could also be factors in determining cytotoxic activity (Salam *et al.*, 2016). The improvement of cytotoxic activity was also suggested to be due to the presence of OH/NH groups, which enabled hydrogen bonding with DNA base pairs (Haque *et al.*, 2015). As part of our on-going studies in the structural elucidation and cytotoxic activity of tin(IV) compounds containing thiosemicarbazones Schiff base (Yusof *et al.*, 2020), herein are described the synthesis of the title dibutyltin(IV) derivative, (I), its single crystal X-ray diffraction analysis and a detailed study of supramolecular association by an analysis of the calculated Hirshfeld surfaces and computational chemistry.

2. Structural commentary

The molecular structure of (I), Sn(C$_{15}$H$_{13}$N$_3$O$_2$S)(C$_4$H$_9$)$_2$ (Fig. 1), comprises a five-coordinate tin centre, being

Table 1
Selected geometric parameters (Å, °).

Sn—S1	2.5598 (7)	Sn—C20	2.140 (3)
Sn—O1	2.1089 (16)	S1—C1	1.747 (3)
Sn—N2	2.212 (2)	N1—C1	1.304 (3)
Sn—C16	2.136 (3)	N2—C2	1.311 (3)
S1—Sn—O1	157.56 (5)	O1—Sn—C16	88.11 (8)
S1—Sn—N2	77.04 (5)	O1—Sn—C20	93.08 (9)
S1—Sn—C16	96.03 (8)	N2—Sn—C16	126.42 (9)
S1—Sn—C20	102.61 (8)	N2—Sn—C20	109.11 (10)
O1—Sn—N2	82.75 (7)	C16—Sn—C20	124.08 (11)

coordinated by a tridentate Schiff base di-anion and two *n*-butyl groups leading to a C$_2$NOS donor set. Selected geometric parameters for (I) are collated in Table 1. While the direct acid analogue for the Schiff base in (I) has yet to be characterized crystallographically, the 4-methoxy analogue is known (Rubčić *et al.*, 2008). Compared to the S1—C1 [1.747 (3) Å], C1—N1 [1.304 (3) Å] and C2—N2 [1.311 (3) Å] bond lengths in (I), the equivalent bonds in the acid are 1.6769 (14), 1.3441 (17) and 1.2798 (18) Å, respectively (Spek, 2020), consistent with elongation, shortening and elongation in (I), respectively, confirming the presence of the thiolate-S1 and imine-N1 atoms. The angles subtended at the tin centre, Table 1, indicate a highly distorted coordination geometry. The angle closest to a *trans* angle is 157.56 (5)°, for S1—Sn—O1, with the next two widest angles being N2—Sn—C16 [126.42 (9)°] and C16—Sn—C20 [124.08 (11)°]. The distortion from the ideal square-pyramidal and trigonal-bipyramidal geometries is quantified by the value of *τ*, with values of 0.0 and 1.0, respectively (Addison *et al.*, 1984). For (I), this
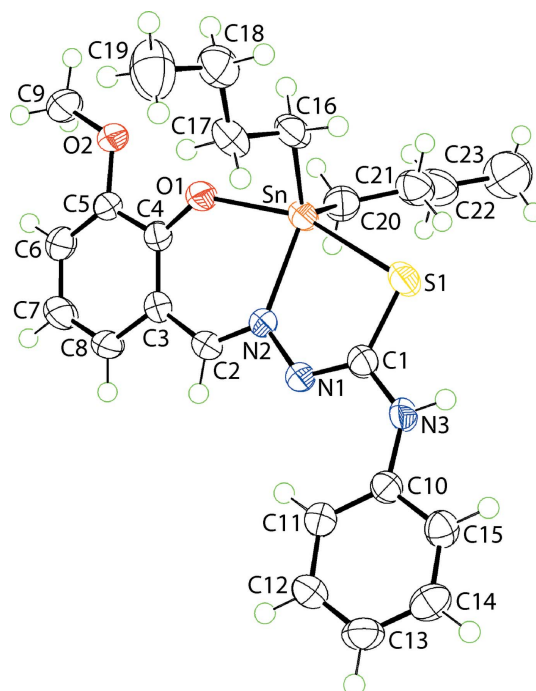

Figure 1
The molecular structure of (I) showing the atom-labelling scheme and displacement ellipsoids at the 70% probability level.

Table 2
Hydrogen-bond geometry (Å, °).

Cg1 is the centroid of the (C10–C15) ring.

$D-H\cdots A$	$D-H$	$H\cdots A$	$D\cdots A$	$D-H\cdots A$
N3—H3$N\cdots$O2^i	0.87 (2)	2.21 (2)	2.990 (3)	150 (2)
C18—H18$A\cdots$Cg1^{ii}	0.99	2.81	3.730 (3)	154

Symmetry codes: (i) $-x+\frac{1}{2}, y+\frac{1}{2}, -z+\frac{1}{2}$; (ii) $x-\frac{1}{2}, -y+\frac{3}{2}, z-\frac{1}{2}$.

computes to 0.52, being almost exactly between the two extreme values.

The N,O,S mode of coordination of the Schiff base di-anion gives rise to the formation of five- and six-membered chelate rings, the acute chelate angles, Table 1; these are partly responsible for the observed distortions in the coordination environment. The former ring, comprising the Sn, S1, N1, N2 and C1 atoms is almost planar, presenting a r.m.s. deviation of 0.0087 Å: atom N3 lies 0.016 (3) Å out of this plane. By contrast, distortions are evident in the six-membered chelate ring, defined by the Sn, O1, N2, C2–C4 atoms. The simplest description for the conformation is that of an envelope with the tin atom lying 0.519 (3) Å out of the plane defined by the remaining five atoms (r.m.s. deviation = 0.0379 Å). The dihedral angle between the five-membered chelate ring and the best plane through the five approximately co-planar atoms of the six-membered chelate ring is 13.59 (12)°, that between the five-membered and N-bound phenyl ring is 6.92 (12)° and that between the peripheral C_6 rings is 19.63 (13)°, highlighting the observation the Schiff base di-anion deviates significantly from co-planarity.

3. Supramolecular features

Conventional hydrogen bonding is noted in the crystal of (I), Table 2. Thus, amine-N—H$\cdots$O(methoxy) hydrogen bonds assemble molecules into a helical, supramolecular chain propagating along the b-axis direction, Fig. 2(a). The only other directional interactions based on an analysis of the points of contact between molecules in the crystal (Spek, 2020), are methylene-C—H$\cdots\pi$(phenyl) interactions. These lead to a supramolecular layer parallel to ($\bar{1}$01), Fig. 2(b). Layers stack without specific interactions between them, Fig. 2(c).

4. Analysis of the Hirshfeld surfaces

The Hirshfeld surface analysis for (I) was conducted to ascertain further information on the supramolecular association between molecules in the crystal, in particular in the interlayer region. The calculated Hirshfeld surface was mapped over the normalized contact distance d_{norm} (McKinnon et al., 2004) and electrostatic potential (Spackman et al., 2008), and the associated two-dimensional fingerprint plots were calculated using Crystal Explorer 17 (Turner et al., 2017) following a literature procedure (Tan et al., 2019). The electrostatic potentials were calculated using the STO-3G basis set at the

Hartree–Fock level of theory. The only red spots observed on the Hirshfeld surface mapped over d_{norm}, Fig. 3, arose as a result of the conventional amine-N3—H3$N\cdots$O2(methoxy) hydrogen bond. This hydrogen bond is also reflected in the
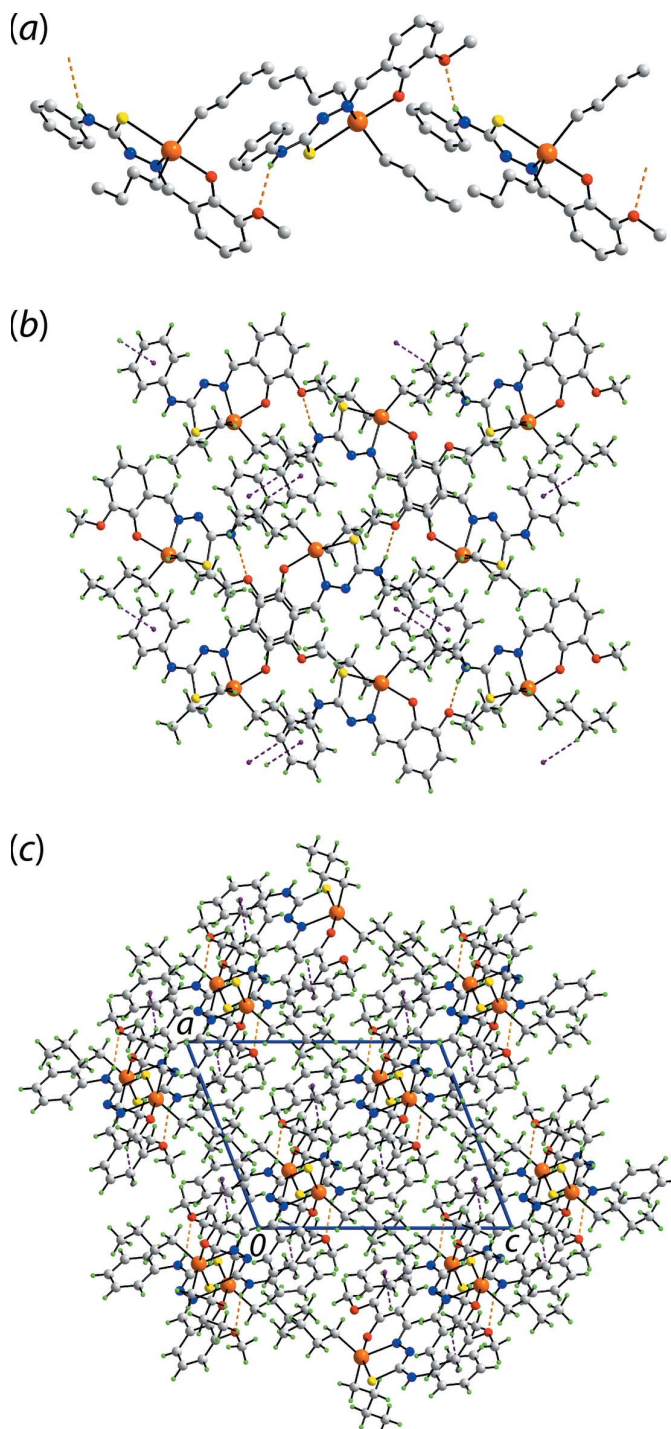
Figure 2
Molecular packing in (I): (a) the helical, supramolecular chain sustained by amine-N—$H\cdots O$(methoxy) hydrogen bonding shown as orange dashed lines (non-participating H atoms omitted), (b) the supramolecular layer parallel to ($\bar{1}$01) whereby the chains of (a) are connected by methylene-C—$H\cdots\pi$(phenyl) interactions shown as purple dashed lines and (c) a view of the unit-cell contents shown in projection down the b-axis direction.

Table 3
A summary of short interatomic contacts (Å) for (I)^a.

Contact	Distance	Symmetry operation
N3—H3N···O2	2.09	$-x + \frac{1}{2}, y + \frac{1}{2}, -z + \frac{1}{2}$
C18—H18A···Cg1	2.81	$x - \frac{1}{2}, -y - \frac{3}{2}, z - \frac{1}{2}$
C22—H22B···Cg1	3.28	$x + \frac{1}{2}, -y + \frac{3}{2}, z - \frac{1}{2}$
H6···H22A	2.32	$-x + \frac{3}{2}, y - \frac{1}{2}, -z + \frac{1}{2}$
H7···H17A	2.32	$-x + 1, -y + 1, -z + 1$

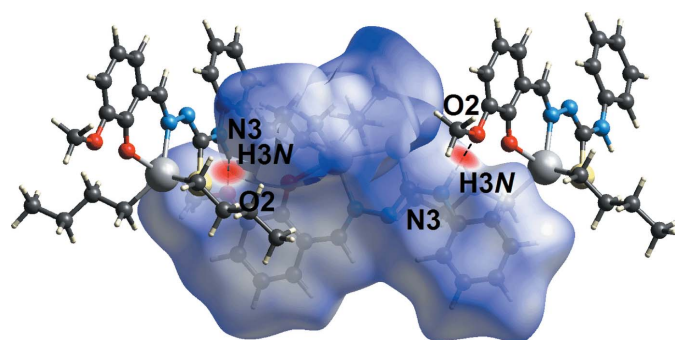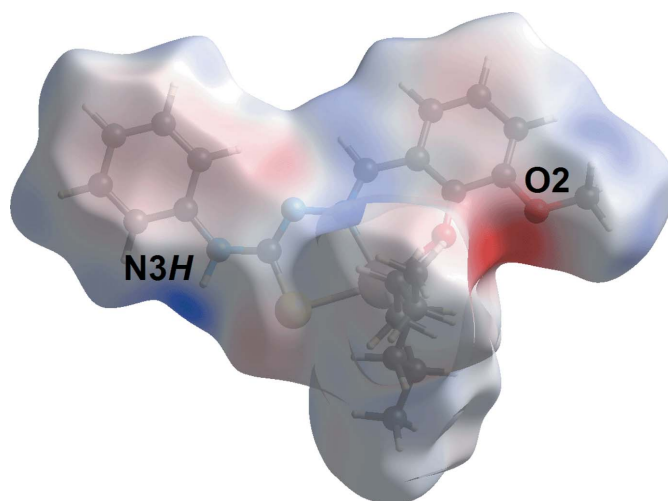Note: (a) The interatomic distances are calculated in *Crystal Explorer 17* (Turner *et al.*, 2017) with the X—H bond lengths adjusted to their neutron values.

Hirshfeld surface mapped over the electrostatic potential, Fig. 4, where the positive electrostatic potential (blue) and negative electrostatic potential (red) regions are evident around the amine-H3N and methoxy-O2 atoms, respectively. Complementing the methylene-C18—H18A···Cg1 contact listed in Table 2, is a longer methylene-C22—H22B···Cg1 contact in the inter-layer region, Table 3. Each interaction is observed as an orange 'hollow' on the Hirshfeld surface mapped over shape-index property, Fig. 5.

The overall two-dimensional fingerprint plot for the Hirshfeld surface of (I) is shown with characteristic pseudo-symmetric wings in the upper left and lower right sides of the d_e and d_i diagonal axes, respectively, in Fig. 6(*a*). The individual H···H, H···C/C···H, H···O/O···H, H···N/N···H and H···S/S···H contacts are illustrated in the delineated fingerprint plots in Fig. 6(*b*)–(*f*), respectively. The percentage contributions for the different interatomic contacts to the Hirshfeld surface are included in Fig. 6. The greatest contribution to the overall Hirshfeld surface is from H···H contacts, *i.e.* 66.2%. The H···H contacts appear as a beak-like distribution tipped at $d_e + d_i \sim 2.4$ Å in Fig. 6(*b*), with the short value corresponding to the H6···H22A and H7···H17A contacts, with details listed in Table 3. The H···C/C···H contacts contribute 17.8% and appear as two sharp-symmetric wings at $d_e + d_i \sim 2.7$ Å, Fig. 6(*c*). This feature reflects the C—H··· π contacts as discussed above. Although H···O/O···H contacts only contribute 5.2% to the overall Hirshfeld surface, they appear as the shortest contacts at $d_e + d_i \sim 2.1$ Å, being 0.6 Å shorter than the sum of their van der Waals radii, Fig. 6(*d*), and reflect the conventional hydrogen bonding leading to the

supramolecular chain. The H···N/N···H and H···S/S···H contacts contribute 4.6 and 4.3%, respectively, to the overall Hirshfeld surface. These contacts are reflected as pseudo-

Figure 4
A view of the Hirshfeld surface mapped over the calculated electrostatic potential for (I) in the range −0.095 to 0.095 a.u.

Figure 5
Views of the Hirshfeld surface for (I) mapped over the shape-index property. The influence of the (*a*) H18A···Cg1 and (*b*) H22B···Cg1 contacts are highlighted by the hollows emphasized by the red circles.
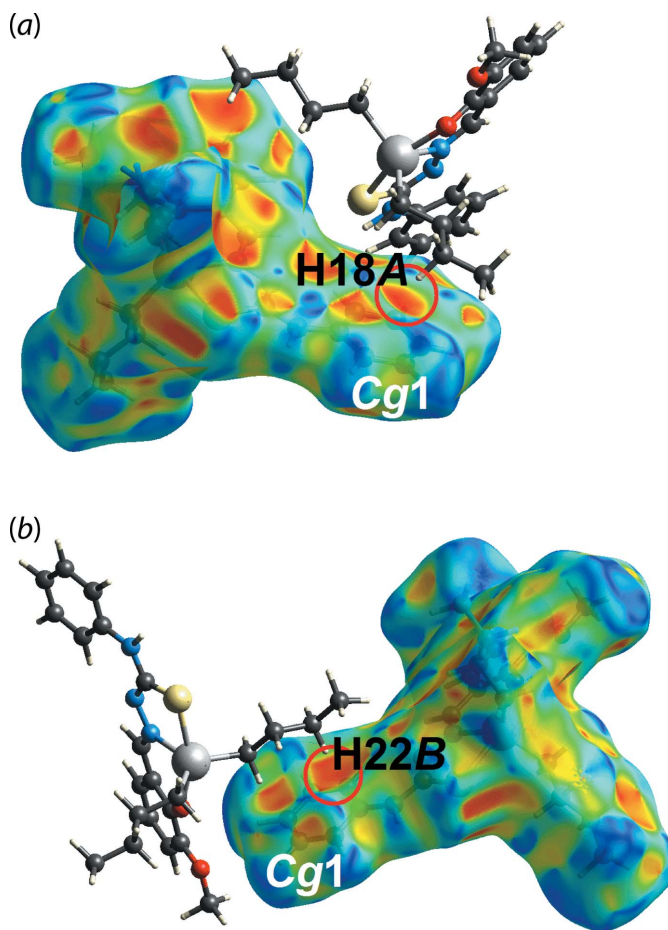

Figure 3
A view of the Hirshfeld surface for (I) mapped over d_{norm} in the range −0.40 to +1.61 arbitrary units, highlighting red spots due to N3—H3N···O2 hydrogen bonds.
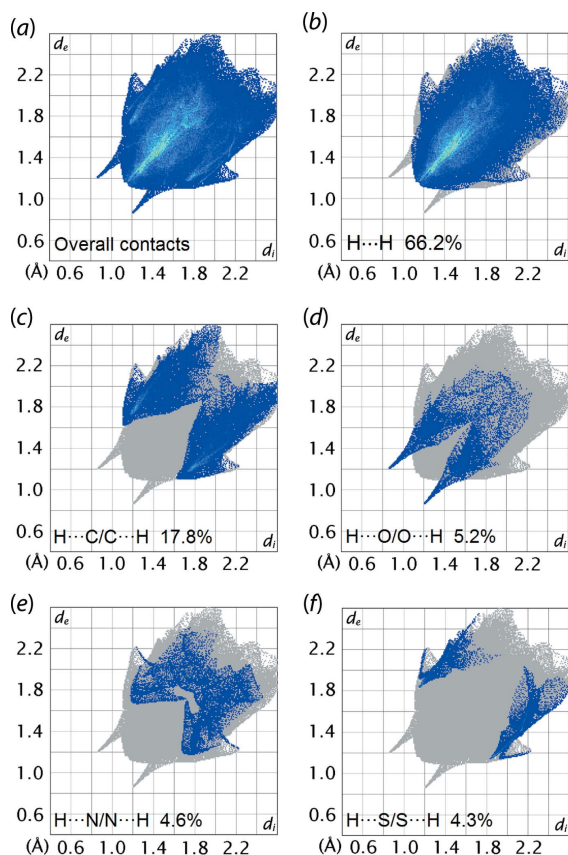
Figure 6
(a) A comparison of the full two-dimensional fingerprint plot for (I) and those delineated into (b) H⋯H, (c) H⋯C/C⋯H, (d) H⋯O/O⋯H, (e) H⋯N/N⋯H and (f) H⋯S/S⋯H contacts.

Table 4
A summary of interaction energies (kJ mol^{-1}) calculated for (I).

Contact	R (Å)	E_{ele}	E_{pol}	E_{dis}	E_{rep}	E_{tot}
Intra-layer region						
N3—H3N⋯O2^i	8.36	−51.6	−10.0	−77.3	74.2	−83.4
H7⋯H17A^{iv} + H9C⋯H11^{iv} + H9C⋯H12^{iv}	7.54	−30.2	−3.3	−88.0	78.5	−62.5
C18—H18A⋯Cg1^{ii}+ H8⋯H21A^v	7.93	−19.5	−2.6	−49.7	43.0	−39.2
H16A⋯H18B^{vi} + H16B⋯H18A^{vi}	10.52	−4.3	−0.1	−24.5	18.6	−14.5
Inter-layer region						
C22—H22B⋯Cg1^{iii}	11.00	−6.8	−1.3	−32.0	16.7	−25.7
H9A⋯H22B^{vii}+ H9A⋯H23A^{vii}	11.46	−2.9	−0.7	−18.7	12.0	−12.6
H14⋯H15^{viii}	15.83	−6.7	−0.7	−14.1	18.3	−8.6
H6⋯H22A^{ix}+ H7⋯H23B^{ix}	12.63	−1.5	−0.4	−11.6	6.0	−8.3
H9A⋯H19C^x	11.27	−1.3	−0.2	−6.4	3.1	−5.2
H12⋯H23A^{xi}	14.28	−2.2	−0.1	−7.2	6.1	−4.9

Symmetry operations: (i) $-x + \frac{1}{2}, y + \frac{1}{2}, -z + \frac{1}{2}$; (ii) $x - \frac{1}{2}, -y + \frac{3}{2}, z - \frac{1}{2}$; (iii) $x + \frac{1}{2}, -y + \frac{3}{2}, z - \frac{1}{2}$; (iv) $-x + 1, -y + 1, -z + 1$; (v) $x + \frac{1}{2}, -y + \frac{3}{2}, z + \frac{1}{2}$; (vi) $-x, -y + 1, -z$; (vii) $-x + 1, -y + 1, -z$; (viii) $-x, -y + 2, -z + 1$; (ix) $-x + \frac{3}{2}, y - \frac{1}{2}, -z + \frac{1}{2}$; (x) $x + 1, y, z$; (xi) $x, y, z + 1$.

5. Computational chemistry

In the present analysis, the pairwise interaction energies between the molecules in the crystal of (I) were calculated using the wave function at the B3LYP/DGDZVP level of theory. The total interaction energies (E_{tot}) as well as individual energy components, namely electrostatic (E_{ele}), polarization (E_{pol}), dispersion (E_{dis}) and exchange-repulsion (E_{rep}) are collated in Table 4. The most significant stabilization energies in the intra-layer region arise from the amine-N3—H3N⋯O2(methoxy) hydrogen bond (E_{tot} = −83.4 kJ mol^{-1}). In addition to the methylene-C18—H18A⋯Cg1 contacts, molecules in the intra-layer region are stabilized by a number of H⋯H contacts, notably H7⋯H17A contacts with a separation of 2.32 Å, Table 3. Therefore, the dispersion term,

mirrored features at $d_e + d_i \sim 3.0$ Å in each of Fig. 6(e) and (f), with the minimum distance being around the sum of their respective van der Waals radii. The other interatomic contacts, i.e. C⋯C and C⋯N/N⋯C, have a negligible effect on the molecular packing and their contributions to the overall Hirshfeld surface are 1.7 and 0.2%, respectively.
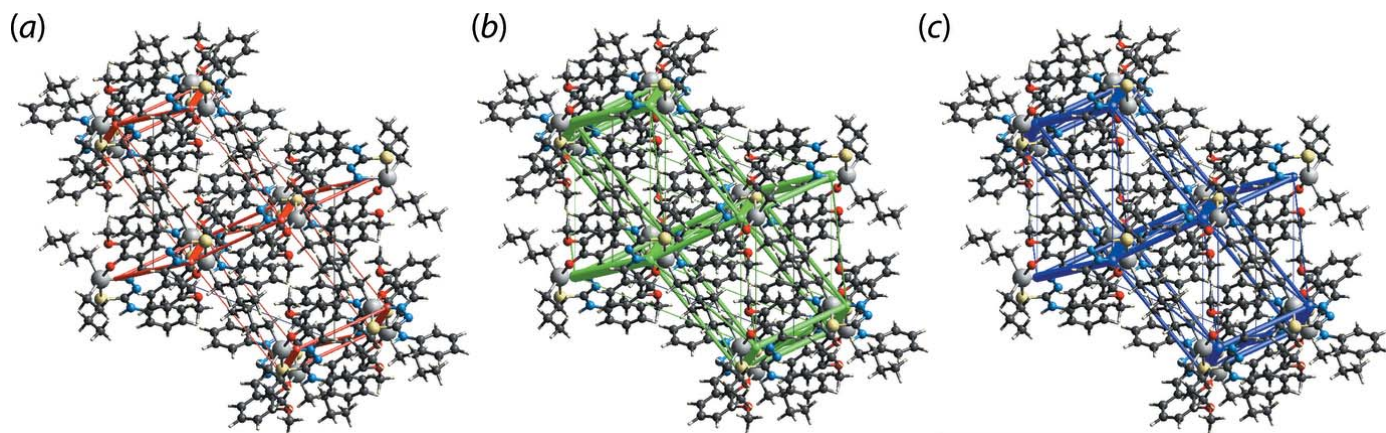

Figure 7
Perspective views of the energy frameworks calculated for (I) showing (a) electrostatic potential force, (b) dispersion force and (c) total energy, each plotted down the b axis. The radii of the cylinders are proportional to the relative magnitudes of the corresponding energies and were adjusted to the same scale factor of 55 with a cut-off value of 5 kJ mol^{-1}.

Table 5
A comparison of key geometric parameters (Å, °) in structures related to (I).

Compound	R, R′	Sn—S	Sn—O1	Sn—N2	S1—Sn—O1	C—Sn—C	τ	Ref.
(I)	nBu, nBu	2.5598 (7)	2.1089 (16)	2.212 (2)	157.56 (5)	124.08 (11)	0.52	This work
(II)	Me, Me	2.4982 (12)	2.085 (3)	2.257 (3)	145.67 (9)	114.82 (18)	0.00	Yusof et al. (2020)
(III)	Ph, Ph	2.5475 (8)	2.0853 (19)	2.176 (3)	161.81 (7)	121.46 (12)	0.60	Yusof et al. (2020)
(IV)^a	nBu, CH$_2$SiM$_3$	2.485 (5)	2.152 (6)	2.184 (6)	159.4 (2)	121.6 (4)	0.60	Xie et al. (2020)
(IV)^b		2.587 (4)	2.063 (6)	2.218 (7)	157.6 (3)	123.8 (4)	0.56	

Notes: (a) major component of the disorder with a site occupancy = 0.527 and (b) minor component with occupancy 0.473.

i.e. E_{dis}, makes the major contribution to the overall inter-action energy in the intra-layer region.

The greatest stabilization energies in the inter-layer region relate to the weak methylene-C22—H22B···Cg1 contact (E_{tot} = −25.7 kJ mol^{-1}) with the remaining intermolecular contacts between molecules being stabilizing H···H contacts. The nature of these contacts leads to the dominance of the E_{dis} component in the molecular packing, Table 4. This observa-tion is also highlighted in the energy framework diagrams of Fig. 7, where the magnitudes of intermolecular energies are represented graphically in the form of cylinders; the wider the cylinder, the greater the energy. The total E_{ele} and E_{dis} components of all pairwise interactions sum to −127.0 and −329.5 kJ mol^{-1}, respectively.

6. Database survey

The crystal structure determination of (I) represents the fourth example of a diorganotin derivative containing the same Schiff base ligand, i.e. RR′Sn(L). Each of the literature structures were reported during 2020, i.e. R = R′ = Me (II) and Ph (III) (Cambridge Structural Database refcodes MUWQED and MUWQAZ, respectively; Yusof et al., 2020) and R = n-Bu and R′ = CH$_2$SiMe$_3$ (IV; CUJHIB; Xie et al., 2020). It is noted that the R = R′ = Ph derivative (III) co-crystallized with one-half mole equivalent of 3-methoxysalicylaldehyde azine (Yusof et al., 2020). Also, two positions were modelled for the tin atom in (IV), with the major component having a site occupancy factor = 0.523 and is designated hereafter as (IVa). Selected geometric parameters for the four structures are collated in Table 5 and an overlay diagram for (I)–(IVa) is shown in Fig. 8. None of the molecules has crystallographic symmetry and all present distorted C$_2$NOS coordination geometries. With the exception of (II), the molecules have intermediate coordination geometries with τ (Addison et al., 1984) ranging from 0.52 in (I) to 0.60 in each of (III) and (IVa). The standout molecule is the dimethyltin derivative (II) which, with τ = 0.00, is well described as having a square-pyramidal geometry. The S1—Sn—O1 angles span a range greater than 15°, i.e. 145.67 (9) in (II) to 161.81 (7)° in (III).

The hydrogen-bonding patterns formed in the crystals of (I)–(IV) are also distinct. Supramolecular helical chains, sustained by amine-H···O(methoxy) hydrogen bonds are found in each of (I) and (IV). However, in (II), the inter-actions leading to a helical chain are of the type amine-H···O(phenoxide). A further distinction is noted in the crystal

of (III) in that dimeric aggregates are formed, featuring amine-N—H···S(thiolate) hydrogen bonding.

7. Synthesis and crystallization

The synthesis of the Schiff base precursor, [2-(2-hydroxy-3-methoxybenzylidene)-N-phenylhydrazine carbothioamide] was according to the procedure described in the literature (Đilović et al., 2008; Kalaivani et al., 2012) with some modifi-cations (Yusof et al., 2020). 4-Phenylthiosemicarbazide (1.67 g, 10 mmol) was dissolved in methanol (40 ml) with stirring and heating (313 K) over a period of 30 min. 2-Hydroxy-3-meth-oxybenzaldehyde (1.52 g, 10 mmol) in methanol (10 ml) was added to the thiosemicarbazide solution and stirred at room temperature for 4 h. Upon cooling, a crystalline product began
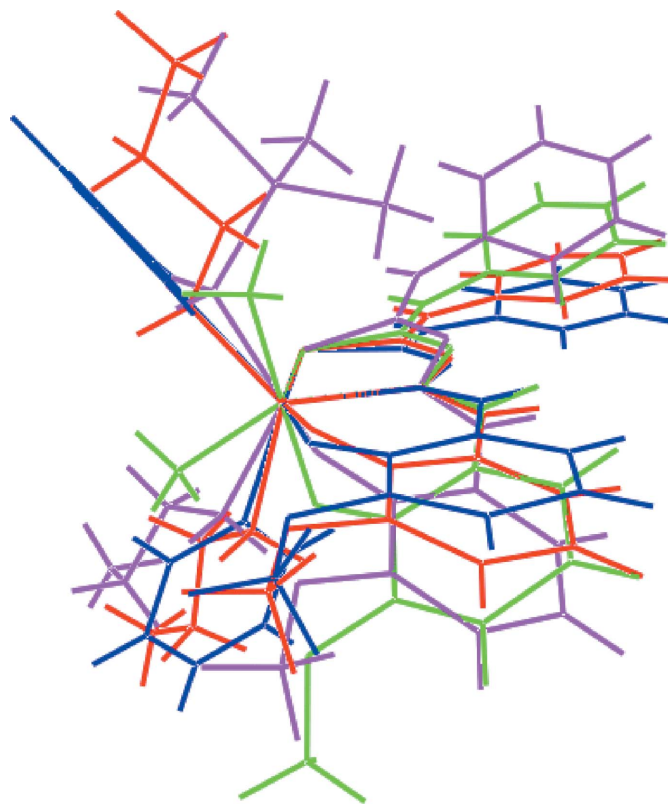

Figure 8
An overlay diagram of (I) red image, (II) green, (III) blue and (IVa) pink. The molecules have been overlapped so that the Sn, S1 and N2 atoms of each molecule are coincident.

Table 6
Experimental details.

Crystal data

Chemical formula	$[Sn(C_4H_9)_2(C_{15}H_{13}N_3O_2S)]$
M_r	532.26
Crystal system, space group	Monoclinic, $P2_1/n$
Temperature (K)	150
a, b, c (Å)	11.2720 (3), 16.1954 (3), 14.2778 (3)
β (°)	111.180 (3)
V (Å^3)	2430.41 (10)
Z	4
Radiation type	Mo $K\alpha$
μ (mm^{-1})	1.16
Crystal size (mm)	$0.15 \times 0.10 \times 0.06$

Data collection

Diffractometer	Rigaku Oxford Diffraction Xcalibur, Eos, Gemini
Absorption correction	Multi-scan (*CrysAlis PRO*; Rigaku OD, 2015)
T_{min}, T_{max}	0.850, 1.000
No. of measured, independent and observed [$I > 2\sigma(I)$] reflections	26999, 5967, 4699
R_{int}	0.051
$(\sin\theta/\lambda)_{max}$ (Å^{-1})	0.689

Refinement

$R[F^2 > 2\sigma(F^2)]$, $wR(F^2)$, S	0.033, 0.076, 1.04
No. of reflections	5967
No. of parameters	277
No. of restraints	1
H-atom treatment	H atoms treated by a mixture of independent and constrained refinement
$\Delta\rho_{max}$, $\Delta\rho_{min}$ (e Å^{-3})	1.63, −0.52

Computer programs: *CrysAlis PRO* (Rigaku OD, 2015), *SHELXT* (Sheldrick, 2015a), *SHELXL2018/3* (Sheldrick, 2015b), *ORTEP-3 for Windows* (Farrugia, 2012), *DIAMOND* (Brandenburg, 2006) and *publCIF* (Westrip, 2010).

to form which was filtered, washed with cold methanol and dried in a desiccator over anhydrous silica gel.

Synthesis of (I): The Schiff base (0.60 g, 2 mmol) was dissolved in a mixture of ethanol:DMF (7:3; 100 ml). Then, Et$_3$N (0.28 ml, 2 mmol) was added dropwise followed by reflux for 2 h. Then, dibutyltin(IV) dichloride (0.61 g, 2 mmol) was added to the mixture followed by reflux for 6 h. The mixture was filtered while hot to remove the [Et$_3$NH]Cl salt that formed and the filtrate was kept at room temperature until bright-yellow crystals appeared. Yield 62%, m.p. 384–385 K. FT–IR (ATR, cm^{-1}): 3322 ν(N—H), 1582 ν(C=N), 1076 ν(N—N), 853 ν(C=S). ^{1}H NMR (CDCl$_3$, 700 MHz) δ: 8.63 (*s*, 1H, NH), 7.54 (*s*, 1H, N—CH), 6.65–7.32 (*m*, 8H, Ar—H), 3.85 (*s*, 3H, O—CH$_3$), *n*-Bu: 1.68 [*t*, 4H, Hα], 1.61 [*m*, 4H, Hβ], 1.34 [*m*, 4H, Hγ], 0.87 [*t*, 6H, Hδ]. ^{13}C NMR (CDCl$_3$, 175 MHz) δ: 162.5 (S$_2$C), 159.0 (C=N), 151.3, 139.6, 128.9, 125.4, 123.1, 120.4, 120.0, 116.9, 116.3, 115.7 (Ar—C), 56.3 (O—CH$_3$), *n*-Bu: 27.5 (Cα), 26.5 (Cβ), 26.0 (Cγ), 13.6 (Cδ).

8. Refinement

Crystal data, data collection and structure refinement details are summarized in Table 6. The carbon-bound H atoms were placed in calculated positions (C—H = 0.95–0.99 Å) and were included in the refinement in the riding-model approximation, with U_{iso}(H) set to 1.2–1.5U_{eq}(C). The N-bound H atom was located in a difference-Fourier map, but was refined with a N—H = 0.88±0.01 Å distance restraint, and with U_{iso}(H) set to 1.2U_{eq}(N). The maximum and minimum residual electron density peaks of 1.63 and 0.52 e Å^{-3}, respectively, were located 0.97 and 0.53 Å from the Sn atom.

References

Addison, A. W., Rao, T. N., Reedijk, J., van Rijn, J. & Verschoor, G. C. (1984). *J. Chem. Soc. Dalton Trans.* pp. 1349–1356.

Brandenburg, K. (2006). *DIAMOND*. Crystal Impact GbR, Bonn, Germany.

Đilović, I., Rubčić, M., Vrdoljak, V., Pavelić, S. K., Kralj, M., Piantanida, I. & Cindrić, M. (2008). *Bioorg. Med. Chem.* **16**, 5189–5198.

Farrugia, L. J. (2012). *J. Appl. Cryst.* **45**, 849–854.

Haque, R. A., Salam, M. A. & Arafath, M. A. (2015). *J. Coord. Chem.* **68**, 2953–2967.

Hu, W., Zhou, W., Xia, C. & Wen, X. (2006). *Bioorg. Med. Chem. Lett.* **16**, 2213–2218.

Kalaivani, P., Prabhakaran, R., Ramachandran, E., Dallemer, F., Paramaguru, G., Renganathan, R., Poornima, P., Vijaya Padma, V. & Natarajan, K. (2012). *Dalton Trans.* **41**, 2486–2499.

Khan, S. A. & Yusuf, M. (2009). *Eur. J. Med. Chem.* **44**, 2270–2274.

Khandani, M., Sedaghat, T., Erfani, N., Haghshenas, M. R. & Khavasi, H. R. (2013). *J. Mol. Struct.* **1037**, 136–143.

Kovala-Demertzi, D., Domopoulou, A., Demertzis, M. A., Valle, G. & Papageorgiou, A. (1997). *J. Inorg. Biochem.* **68**, 147–155.

Li, M. X., Zhang, D., Zhang, L. Z., Niu, J. Y. & Ji, B. S. (2011). *J. Organomet. Chem.* **696**, 852–858.

Liu, K., Yan, H., Chang, G., Li, Z., Niu, M. & Hong, M. (2017). *Inorg. Chim. Acta*, **464**, 137–146.

McKinnon, J. J., Spackman, M. A. & Mitchell, A. S. (2004). *Acta Cryst.* B**60**, 627–668.

Palanimuthu, D., Poon, R., Sahni, S., Anjum, R., Hibbs, D., Lin, H. Y., Bernhardt, P. V., Kalinowski, D. S. & Richardson, D. R. (2017). *Eur. J. Med. Chem.* **139**, 612–632.

Parrilha, G. L., da Silva, J. G., Gouveia, L. F., Gasparoto, A. K., Dias, R. P., Rocha, W. R., Santos, D. A., Speziali, N. L. & Beraldo, H. (2011). *Eur. J. Med. Chem.* **46**, 1473–1482.

Pavan, F. R., Maia, P. I. da S., Leite, S. R. A., Deflon, V. M., Batista, A. A., Sato, D. N., Franzblau, S. G. & Leite, C. Q. F. (2010). *Eur. J. Med. Chem.* **45**, 1898–1905.

Rigaku OD (2015). *CrysAlis PRO*. Agilent Technologies Inc., Santa Clara, CA, USA.

Rubčić, M., Đilović, I., Cindrić, M. & Matković-Čalogović, D. (2008). *Acta Cryst.* C**64**, o570–o573.

Salam, M. A., Hussein, M. A., Ramli, I. & Islam, S. (2016). *J. Organomet. Chem.* **813**, 71–77.

Sheldrick, G. M. (2015a). *Acta Cryst.* A**71**, 3–8.

Sheldrick, G. M. (2015b). *Acta Cryst.* C**71**, 3–8.

Singh, H. L., Singh, J. B. & Bhanuka, S. (2016). *Res. Chem. Intermed.* **42**, 997–1015.

Spackman, M. A., McKinnon, J. J. & Jayatilaka, D. (2008). *CrystEngComm*, **10**, 377–388.

Spek, A. L. (2020). *Acta Cryst.* E**76**, 1–11.

Tan, S. L., Jotani, M. M. & Tiekink, E. R. T. (2019). *Acta Cryst.* E**75**, 308–318.

Turner, M. J., Mckinnon, J. J., Wolff, S. K., Grimwood, D. J., Spackman, P. R., Jayatilaka, D. & Spackman, M. A. (2017). *Crystal Explorer 17*. The University of Western Australia.

Westrip, S. P. (2010). *J. Appl. Cryst.* **43**, 920–925.

Wiecek, J., Dokorou, V., Ciunik, Z. & Kovala-Demertzi, D. (2009). *Polyhedron*, **28**, 3298–3304.

Xie, B., Yao, H., Liao, Q.-H., Deng, R.-H., Lin, S. & Yan, Z.-H. (2020). *Chin. J. Inorg. Chem.* **36**, 819–826.

Yusof, E. N. M., Page, A. J., Sakoff, J. A., Simone, M. I., Veerakumarasivam, A., Tiekink, E. R. T. & Ravoof, T. B. S. A. (2020). *Polyhedron*, **189** article No. 114729.

Di-*n*-butyl[*N*′-(3-methoxy-2-oxidobenzylidene)-*N*-phenylcarbamohydrazono-thioato]tin(IV): crystal structure, Hirshfeld surface analysis and computational study

Enis Nadia Md Yusof, Huey Chong Kwong, Thiruventhan Karunakaran, Thahira B. S. A. Ravoof and Edward R. T. Tiekink

Computing details

Data collection: *CrysAlis PRO* (Rigaku OD, 2015); cell refinement: *CrysAlis PRO* (Rigaku OD, 2015); data reduction: *CrysAlis PRO* (Rigaku OD, 2015); program(s) used to solve structure: SHELXT (Sheldrick, 2015*a*); program(s) used to refine structure: *SHELXL2018/3* (Sheldrick, 2015*b*); molecular graphics: *ORTEP-3 for Windows* (Farrugia, 2012), *DIAMOND* (Brandenburg, 2006); software used to prepare material for publication: *publCIF* (Westrip, 2010).

Di-*n*-butyl[*N*′-(3-methoxy-2-oxidobenzylidene)-*N*-phenylcarbamohydrazonothioato]tin(IV)

Crystal data

$[Sn(C_4H_9)_2(C_{15}H_{13}N_3O_2S)]$	$F(000) = 1088$
$M_r = 532.26$	$D_x = 1.455$ Mg m^{-3}
Monoclinic, $P2_1/n$	Mo $K\alpha$ radiation, $\lambda = 0.71073$ Å
$a = 11.2720$ (3) Å	Cell parameters from 9470 reflections
$b = 16.1954$ (3) Å	$\theta = 3.8$–$28.9°$
$c = 14.2778$ (3) Å	$\mu = 1.16$ mm^{-1}
$\beta = 111.180$ (3)°	$T = 150$ K
$V = 2430.41$ (10) Å^3	Prism, yellow
$Z = 4$	$0.15 \times 0.10 \times 0.06$ mm

Data collection

Rigaku Oxford Diffraction Xcalibur, Eos, Gemini diffractometer	$T_{min} = 0.850$, $T_{max} = 1.000$
	26999 measured reflections
	5967 independent reflections
Radiation source: fine-focus sealed X-ray tube, Enhance (Mo) X-ray Source	4699 reflections with $I > 2\sigma(I)$
Graphite monochromator	$R_{int} = 0.051$
Detector resolution: 16.1952 pixels mm^{-1}	$\theta_{max} = 29.3°$, $\theta_{min} = 3.8°$
ω scans	$h = -15 \rightarrow 14$
Absorption correction: multi-scan (CrysAlis PRO; Rigaku OD, 2015)	$k = -21 \rightarrow 22$
	$l = -19 \rightarrow 18$

Refinement

Refinement on F^2	$S = 1.03$
Least-squares matrix: full	5967 reflections
$R[F^2 > 2\sigma(F^2)] = 0.033$	277 parameters
$wR(F^2) = 0.076$	1 restraint

Primary atom site location: structure-invariant direct methods
Secondary atom site location: difference Fourier map
Hydrogen site location: mixed

H atoms treated by a mixture of independent and constrained refinement
$w = 1/[\sigma^2(F_o^2) + (0.0297P)^2 + 1.1545P]$
where $P = (F_o^2 + 2F_c^2)/3$
$(\Delta/\sigma)_{max} = 0.001$
$\Delta\rho_{max} = 1.63$ e Å^{-3}
$\Delta\rho_{min} = -0.52$ e Å^{-3}

Special details

Geometry. All esds (except the esd in the dihedral angle between two l.s. planes) are estimated using the full covariance matrix. The cell esds are taken into account individually in the estimation of esds in distances, angles and torsion angles; correlations between esds in cell parameters are only used when they are defined by crystal symmetry. An approximate (isotropic) treatment of cell esds is used for estimating esds involving l.s. planes.

Fractional atomic coordinates and isotropic or equivalent isotropic displacement parameters (Å²)

	x	*y*	*z*	U_{iso}*/U_{eq}
Sn	0.30782 (2)	0.63922 (2)	0.20843 (2)	0.02658 (7)
S1	0.17922 (7)	0.76839 (5)	0.21316 (5)	0.03737 (18)
O1	0.41536 (16)	0.53123 (10)	0.26242 (13)	0.0299 (4)
O2	0.55992 (16)	0.40842 (10)	0.25269 (13)	0.0279 (4)
N1	0.3367 (2)	0.74015 (12)	0.40760 (15)	0.0271 (5)
N2	0.38235 (19)	0.67314 (12)	0.36939 (15)	0.0245 (5)
N3	0.1999 (2)	0.85096 (13)	0.37649 (16)	0.0278 (5)
H3N	0.142 (2)	0.8768 (15)	0.3282 (15)	0.033*
C1	0.2476 (2)	0.78406 (15)	0.34279 (18)	0.0267 (6)
C2	0.4807 (2)	0.63876 (15)	0.43827 (19)	0.0266 (5)
H2	0.507201	0.663195	0.503089	0.032*
C3	0.5533 (2)	0.56903 (15)	0.42817 (18)	0.0253 (5)
C4	0.5195 (2)	0.51976 (14)	0.34156 (18)	0.0231 (5)
C5	0.5993 (2)	0.45193 (15)	0.34154 (18)	0.0240 (5)
C6	0.7057 (2)	0.43422 (16)	0.4235 (2)	0.0315 (6)
H6	0.758465	0.388936	0.421749	0.038*
C7	0.7367 (3)	0.48344 (17)	0.5104 (2)	0.0373 (7)
H7	0.809490	0.470558	0.567769	0.045*
C8	0.6629 (2)	0.54928 (16)	0.51260 (19)	0.0320 (6)
H8	0.685130	0.582370	0.571384	0.038*
C9	0.6339 (3)	0.33893 (18)	0.2478 (2)	0.0414 (7)
H9A	0.720214	0.356915	0.256299	0.062*
H9B	0.595020	0.311870	0.182395	0.062*
H9C	0.637687	0.299962	0.301309	0.062*
C10	0.2229 (2)	0.87931 (15)	0.47493 (19)	0.0246 (5)
C11	0.3071 (3)	0.84289 (16)	0.5628 (2)	0.0321 (6)
H11	0.356486	0.796350	0.559100	0.039*
C12	0.3174 (3)	0.87544 (17)	0.6549 (2)	0.0355 (7)
H12	0.374328	0.850489	0.714380	0.043*
C13	0.2475 (3)	0.94306 (17)	0.6629 (2)	0.0353 (6)
H13	0.254424	0.963702	0.726972	0.042*
C14	0.1671 (3)	0.98029 (17)	0.5762 (2)	0.0331 (6)

H14	0.119945	1.027809	0.580593	0.040*
C15	0.1547 (2)	0.94894 (16)	0.4831 (2)	0.0286 (6)
H15	0.099062	0.975153	0.424064	0.034*
C16	0.1475 (2)	0.56202 (17)	0.13464 (19)	0.0320 (6)
H16A	0.073373	0.597705	0.099569	0.038*
H16B	0.165615	0.529157	0.082891	0.038*
C17	0.1111 (3)	0.50319 (18)	0.2027 (2)	0.0368 (7)
H17A	0.078865	0.535372	0.247468	0.044*
H17B	0.187726	0.472697	0.245367	0.044*
C18	0.0095 (3)	0.44156 (18)	0.1427 (2)	0.0408 (7)
H18A	−0.067397	0.472273	0.101010	0.049*
H18B	0.041312	0.410471	0.096902	0.049*
C19	−0.0267 (3)	0.3812 (2)	0.2085 (3)	0.0630 (11)
H19A	0.046823	0.346452	0.244721	0.095*
H19B	−0.096854	0.346334	0.166641	0.095*
H19C	−0.053386	0.411610	0.256866	0.095*
C20	0.4355 (3)	0.68370 (17)	0.1396 (2)	0.0348 (6)
H20A	0.510109	0.708354	0.192719	0.042*
H20B	0.466511	0.635693	0.112094	0.042*
C21	0.3833 (3)	0.74679 (18)	0.0563 (2)	0.0385 (7)
H21A	0.345417	0.793150	0.081061	0.046*
H21B	0.314902	0.720923	−0.000729	0.046*
C22	0.4850 (3)	0.7805 (2)	0.0194 (2)	0.0487 (8)
H22A	0.555087	0.804035	0.077308	0.058*
H22B	0.520427	0.734251	−0.007521	0.058*
C23	0.4367 (5)	0.8464 (2)	−0.0612 (3)	0.0684 (11)
H23A	0.360725	0.826100	−0.115308	0.103*
H23B	0.502935	0.859307	−0.088338	0.103*
H23C	0.415227	0.896385	−0.031958	0.103*

Atomic displacement parameters (Å²)

	U^{11}	U^{22}	U^{33}	U^{12}	U^{13}	U^{23}
Sn	0.02994 (10)	0.02799 (11)	0.01860 (10)	0.00565 (7)	0.00492 (7)	−0.00006 (7)
S1	0.0463 (4)	0.0399 (4)	0.0204 (3)	0.0194 (3)	0.0054 (3)	0.0010 (3)
O1	0.0297 (9)	0.0269 (9)	0.0246 (9)	0.0067 (7)	−0.0003 (7)	−0.0032 (7)
O2	0.0323 (9)	0.0233 (9)	0.0253 (9)	0.0031 (7)	0.0069 (8)	−0.0037 (7)
N1	0.0342 (12)	0.0242 (11)	0.0205 (11)	0.0081 (9)	0.0068 (9)	−0.0008 (9)
N2	0.0308 (11)	0.0213 (10)	0.0201 (11)	0.0058 (9)	0.0076 (9)	−0.0001 (8)
N3	0.0339 (12)	0.0270 (12)	0.0213 (11)	0.0122 (9)	0.0086 (9)	0.0040 (9)
C1	0.0315 (13)	0.0262 (13)	0.0229 (13)	0.0041 (11)	0.0104 (11)	0.0024 (10)
C2	0.0313 (13)	0.0267 (13)	0.0191 (12)	0.0018 (11)	0.0059 (10)	−0.0007 (10)
C3	0.0277 (12)	0.0239 (13)	0.0221 (13)	0.0028 (10)	0.0065 (10)	0.0027 (10)
C4	0.0235 (12)	0.0219 (12)	0.0223 (13)	0.0006 (10)	0.0062 (10)	0.0014 (10)
C5	0.0275 (12)	0.0211 (12)	0.0225 (13)	−0.0022 (10)	0.0079 (10)	−0.0009 (10)
C6	0.0323 (14)	0.0263 (14)	0.0337 (15)	0.0081 (11)	0.0093 (12)	0.0002 (11)
C7	0.0353 (15)	0.0399 (16)	0.0259 (15)	0.0094 (12)	−0.0019 (12)	−0.0005 (12)
C8	0.0353 (14)	0.0299 (14)	0.0224 (13)	0.0051 (11)	0.0004 (11)	−0.0045 (11)

C9	0.0522 (18)	0.0321 (15)	0.0359 (17)	0.0140 (13)	0.0109 (14)	−0.0065 (13)
C10	0.0283 (12)	0.0249 (13)	0.0225 (13)	0.0001 (10)	0.0114 (10)	0.0011 (10)
C11	0.0428 (16)	0.0264 (14)	0.0266 (14)	0.0062 (11)	0.0119 (12)	0.0015 (11)
C12	0.0498 (17)	0.0332 (15)	0.0219 (14)	0.0005 (13)	0.0108 (12)	0.0007 (11)
C13	0.0468 (17)	0.0341 (15)	0.0292 (15)	−0.0028 (13)	0.0187 (13)	−0.0071 (12)
C14	0.0334 (14)	0.0320 (14)	0.0391 (16)	0.0016 (12)	0.0193 (13)	−0.0049 (12)
C15	0.0268 (13)	0.0303 (14)	0.0295 (14)	0.0034 (11)	0.0111 (11)	0.0024 (11)
C16	0.0296 (13)	0.0392 (15)	0.0215 (13)	0.0030 (12)	0.0024 (11)	0.0001 (12)
C17	0.0366 (15)	0.0454 (17)	0.0230 (14)	0.0027 (13)	0.0041 (11)	0.0043 (12)
C18	0.0341 (15)	0.0447 (17)	0.0377 (17)	0.0015 (13)	0.0059 (13)	0.0018 (14)
C19	0.048 (2)	0.059 (2)	0.071 (3)	−0.0058 (17)	0.0099 (19)	0.0203 (19)
C20	0.0392 (15)	0.0353 (15)	0.0329 (16)	0.0039 (12)	0.0168 (13)	−0.0008 (12)
C21	0.0435 (16)	0.0439 (17)	0.0300 (15)	0.0005 (13)	0.0155 (13)	−0.0009 (13)
C22	0.059 (2)	0.056 (2)	0.0358 (17)	−0.0094 (17)	0.0237 (16)	−0.0045 (15)
C23	0.106 (3)	0.060 (2)	0.055 (2)	−0.008 (2)	0.048 (2)	0.0049 (19)

Geometric parameters (Å, º)

Sn—S1	2.5598 (7)	C11—H11	0.9500
Sn—O1	2.1089 (16)	C12—C13	1.378 (4)
Sn—N2	2.212 (2)	C12—H12	0.9500
Sn—C16	2.136 (3)	C13—C14	1.381 (4)
Sn—C20	2.140 (3)	C13—H13	0.9500
S1—C1	1.747 (3)	C14—C15	1.382 (4)
O1—C4	1.316 (3)	C14—H14	0.9500
O2—C5	1.377 (3)	C15—H15	0.9500
O2—C9	1.417 (3)	C16—C17	1.519 (4)
N1—C1	1.304 (3)	C16—H16A	0.9900
N1—N2	1.394 (3)	C16—H16B	0.9900
N2—C2	1.311 (3)	C17—C18	1.528 (4)
N3—C1	1.371 (3)	C17—H17A	0.9900
N3—C10	1.411 (3)	C17—H17B	0.9900
N3—H3N	0.866 (10)	C18—C19	1.510 (4)
C2—C3	1.432 (3)	C18—H18A	0.9900
C2—H2	0.9500	C18—H18B	0.9900
C3—C4	1.404 (3)	C19—H19A	0.9800
C3—C8	1.416 (3)	C19—H19B	0.9800
C4—C5	1.420 (3)	C19—H19C	0.9800
C5—C6	1.370 (3)	C20—C21	1.516 (4)
C6—C7	1.408 (4)	C20—H20A	0.9900
C6—H6	0.9500	C20—H20B	0.9900
C7—C8	1.359 (4)	C21—C22	1.525 (4)
C7—H7	0.9500	C21—H21A	0.9900
C8—H8	0.9500	C21—H21B	0.9900
C9—H9A	0.9800	C22—C23	1.519 (5)
C9—H9B	0.9800	C22—H22A	0.9900
C9—H9C	0.9800	C22—H22B	0.9900
C10—C15	1.393 (3)	C23—H23A	0.9800

C10—C11	1.400 (4)	C23—H23B	0.9800
C11—C12	1.382 (4)	C23—H23C	0.9800
S1—Sn—O1	157.56 (5)	C11—C12—H12	119.1
S1—Sn—N2	77.04 (5)	C12—C13—C14	118.8 (3)
S1—Sn—C16	96.03 (8)	C12—C13—H13	120.6
S1—Sn—C20	102.61 (8)	C14—C13—H13	120.6
O1—Sn—N2	82.75 (7)	C13—C14—C15	120.5 (3)
O1—Sn—C16	88.11 (8)	C13—C14—H14	119.8
O1—Sn—C20	93.08 (9)	C15—C14—H14	119.8
N2—Sn—C16	126.42 (9)	C14—C15—C10	120.7 (2)
N2—Sn—C20	109.11 (10)	C14—C15—H15	119.6
C16—Sn—C20	124.08 (11)	C10—C15—H15	119.6
C1—S1—Sn	96.29 (8)	C17—C16—Sn	115.28 (17)
C4—O1—Sn	130.37 (15)	C17—C16—H16A	108.5
C5—O2—C9	116.9 (2)	Sn—C16—H16A	108.5
C1—N1—N2	116.5 (2)	C17—C16—H16B	108.5
C2—N2—N1	111.6 (2)	Sn—C16—H16B	108.5
C2—N2—Sn	125.07 (17)	H16A—C16—H16B	107.5
N1—N2—Sn	123.00 (14)	C16—C17—C18	111.8 (2)
C1—N3—C10	130.7 (2)	C16—C17—H17A	109.2
C1—N3—H3N	112.2 (19)	C18—C17—H17A	109.2
C10—N3—H3N	116.8 (19)	C16—C17—H17B	109.2
N1—C1—N3	118.8 (2)	C18—C17—H17B	109.2
N1—C1—S1	127.2 (2)	H17A—C17—H17B	107.9
N3—C1—S1	114.06 (17)	C19—C18—C17	113.0 (3)
N2—C2—C3	128.2 (2)	C19—C18—H18A	109.0
N2—C2—H2	115.9	C17—C18—H18A	109.0
C3—C2—H2	115.9	C19—C18—H18B	109.0
C4—C3—C8	119.8 (2)	C17—C18—H18B	109.0
C4—C3—C2	123.6 (2)	H18A—C18—H18B	107.8
C8—C3—C2	116.5 (2)	C18—C19—H19A	109.5
O1—C4—C3	123.4 (2)	C18—C19—H19B	109.5
O1—C4—C5	118.6 (2)	H19A—C19—H19B	109.5
C3—C4—C5	118.0 (2)	C18—C19—H19C	109.5
C6—C5—O2	124.8 (2)	H19A—C19—H19C	109.5
C6—C5—C4	121.4 (2)	H19B—C19—H19C	109.5
O2—C5—C4	113.7 (2)	C21—C20—Sn	116.88 (19)
C5—C6—C7	119.7 (2)	C21—C20—H20A	108.1
C5—C6—H6	120.1	Sn—C20—H20A	108.1
C7—C6—H6	120.1	C21—C20—H20B	108.1
C8—C7—C6	120.4 (2)	Sn—C20—H20B	108.1
C8—C7—H7	119.8	H20A—C20—H20B	107.3
C6—C7—H7	119.8	C20—C21—C22	112.7 (3)
C7—C8—C3	120.7 (2)	C20—C21—H21A	109.1
C7—C8—H8	119.7	C22—C21—H21A	109.1
C3—C8—H8	119.7	C20—C21—H21B	109.1
O2—C9—H9A	109.5	C22—C21—H21B	109.1

O2—C9—H9B	109.5	H21A—C21—H21B	107.8
H9A—C9—H9B	109.5	C23—C22—C21	113.9 (3)
O2—C9—H9C	109.5	C23—C22—H22A	108.8
H9A—C9—H9C	109.5	C21—C22—H22A	108.8
H9B—C9—H9C	109.5	C23—C22—H22B	108.8
C15—C10—C11	118.8 (2)	C21—C22—H22B	108.8
C15—C10—N3	116.0 (2)	H22A—C22—H22B	107.7
C11—C10—N3	125.2 (2)	C22—C23—H23A	109.5
C12—C11—C10	119.2 (3)	C22—C23—H23B	109.5
C12—C11—H11	120.4	H23A—C23—H23B	109.5
C10—C11—H11	120.4	C22—C23—H23C	109.5
C13—C12—C11	121.9 (3)	H23A—C23—H23C	109.5
C13—C12—H12	119.1	H23B—C23—H23C	109.5
C1—N1—N2—C2	173.0 (2)	O1—C4—C5—O2	4.0 (3)
C1—N1—N2—Sn	−1.2 (3)	C3—C4—C5—O2	−178.7 (2)
N2—N1—C1—N3	−179.6 (2)	O2—C5—C6—C7	179.8 (2)
N2—N1—C1—S1	−0.2 (4)	C4—C5—C6—C7	0.7 (4)
C10—N3—C1—N1	−6.2 (4)	C5—C6—C7—C8	−1.3 (4)
C10—N3—C1—S1	174.3 (2)	C6—C7—C8—C3	0.6 (5)
Sn—S1—C1—N1	1.1 (3)	C4—C3—C8—C7	0.7 (4)
Sn—S1—C1—N3	−179.43 (18)	C2—C3—C8—C7	179.1 (3)
N1—N2—C2—C3	180.0 (2)	C1—N3—C10—C15	−177.9 (3)
Sn—N2—C2—C3	−6.0 (4)	C1—N3—C10—C11	1.8 (4)
N2—C2—C3—C4	−7.4 (4)	C15—C10—C11—C12	1.8 (4)
N2—C2—C3—C8	174.2 (3)	N3—C10—C11—C12	−177.9 (3)
Sn—O1—C4—C3	26.6 (4)	C10—C11—C12—C13	−0.2 (4)
Sn—O1—C4—C5	−156.24 (18)	C11—C12—C13—C14	−1.5 (4)
C8—C3—C4—O1	175.9 (2)	C12—C13—C14—C15	1.6 (4)
C2—C3—C4—O1	−2.4 (4)	C13—C14—C15—C10	0.0 (4)
C8—C3—C4—C5	−1.2 (4)	C11—C10—C15—C14	−1.7 (4)
C2—C3—C4—C5	−179.5 (2)	N3—C10—C15—C14	178.0 (2)
C9—O2—C5—C6	1.9 (4)	Sn—C16—C17—C18	−171.27 (19)
C9—O2—C5—C4	−179.0 (2)	C16—C17—C18—C19	178.9 (3)
O1—C4—C5—C6	−176.8 (2)	Sn—C20—C21—C22	174.5 (2)
C3—C4—C5—C6	0.5 (4)	C20—C21—C22—C23	−177.7 (3)

Hydrogen-bond geometry (Å, º)

*Cg*1 is the centroid of the (C10–C15) ring.

D—H···*A*	*D*—H	H···*A*	*D*···*A*	*D*—H···*A*
N3—H3*N*···O2[i]	0.87 (2)	2.21 (2)	2.990 (3)	150 (2)
C18—H18*A*···*Cg*1[ii]	0.99	2.81	3.730 (3)	154

Symmetry codes: (i) −*x*+1/2, *y*+1/2, −*z*+1/2; (ii) *x*−1/2, −*y*+3/2, *z*−1/2.